Journal of Materials Chemistry C

PAPER

View Article Online
View Journal | View Issue

Cite this: J. Mater. Chem. C, 2018, 6, 3352

Multiple spin phases in a switchable Fe(II) complex: polymorphism and symmetry breaking effects†

Hao Hang,[a] Bin Fei,[a] Xiu Qin Chen,[a] Ming Liang Tong,[b] Vadim Ksenofontov,[c] Il'ya A. Gural'skiy*[d] and Xin Bao*[a]

Received 9th November 2017,
Accepted 19th February 2018

DOI: 10.1039/c7tc05111e

rsc.li/materials-c

Polymorphism in spin-crossover (SCO) compounds allows accessing additional forms of switchable materials with diverse transition properties. We have prepared three polymorphs of a new complex $[FeL_{Br}(dca)_2]$, where L_{Br} is *N*,*N*′-bis[(5-bromo-2-pyridyl)methyl]ethane-1,2-diamine and dca is dicyanamide. They display different SCO properties: the α-form displays a hysteretic one-step switch centered at 134 K, the β-form undergoes hysteretic two-step spin transition with a plateau ($T_{1/2}$ = 153 and 144 K) and the γ-form remains high spin (HS) over the whole temperature region. The kinetic origin of the hysteresis loop was demonstrated in temperature rate dependent magnetic measurements. Spin transition in the α-form is accompanied by symmetry breaking from a single Fe(II) site in the HS state to two distinct Fe(II) sites in the low spin (LS) state. In the β-form, the single crystal XRD has revealed a re-entrant symmetry change associated with the stepwise transition, with an ordered HS–LS alternating arrangement in the temperature plateau range. The corresponding Mössbauer study demonstrates a complicated evolution of spin transitions in the β-form through three different spin phases within different temperature regions.

Introduction

Polymorphism, as the ability of solid materials to exist in more than one crystal form, opens a pathway to numerous functionally attractive forms of different compounds. Polymorphism in organic compounds is mostly important in applications in pharmaceutical chemistry when two polymorphs of one drug can have a different solubility[1] or compressibility to form pellets.[2] In biochemistry, conformational variety is frequently responsible for the polymorphism in biopolymers.[3] In materials chemistry, the polymorphs also have different functional properties, *e.g.* magnetic, superconductive *etc.*[4]

Among many metal based functional materials, the so-called spin crossover (SCO) complexes have attracted attention by their fascinating ability to be reversibly changed between high spin (HS) and low spin (LS) states, and this consequently changes all their associated physical properties.[5] Different means have been applied to switch the spin states including temperature, light irradiation, pressure, magnetic field, guest effect *etc.*[6,7] These switchable materials have given rise to many applications such as chemical sensors,[8] electronic[9,10] and thermochromic elements.[11] Even though the SCO itself occurs within a metal center and is mostly affected by the first coordination sphere, the lattice contribution still plays an important (and sometimes even a crucial) role in defining the spin state behavior. These lattice effects are also responsible for transmitting communication between metal centers, leading to the so-called cooperativity of the spin transition (ST). Strongly cooperative SCO systems are among the most desired especially those displaying hysteretic ST near technologically attractive room temperatures.

The effect of polymorphism in spin crossover complexes deserves particular attention, since it offers a facile opportunity to obtain many attractive SCO complexes with additional functionalities from the same set of building blocks.[12] It also allows investigating the influence of molecular packing and supramolecular interactions that are crucial for understanding the cooperativity. Sequential single crystal to single crystal transformation through desolvation has been reported as a rational approach to obtain SCO polymorphs.[13–15] In the case of

[a] School of Chemical Engineering, Nanjing University of Science and Technology, 210094 Nanjing, P. R. China. E-mail: baox199@126.com
[b] Key Laboratory of Bioinorganic and Synthetic Chemistry of Ministry of Education, School of Chemistry, Sun Yat-Sen University, 510275 Guangzhou, P. R. China
[c] Institute of Inorganic and Analytical Chemistry, Johannes Gutenberg University of Mainz, Duesbergweg 10-14, 55099 Mainz, Germany
[d] Department of Chemistry, Taras Shevchenko National University of Kyiv, 64 Volodymyrska St., Kyiv 01601, Ukraine. E-mail: illia.guralskyi@univ.kiev.ua

† Electronic supplementary information (ESI) available: PXRD patterns, IR spectra, additional magnetic and structural figures. CCDC 1582828–1582833 and 1816546. For ESI and crystallographic data in CIF or another electronic format see DOI: 10.1039/c7tc05111e

the solution chemistry, upon crystallization certain stimuli can facilitate the formation of a given polymorph, like the solvent, temperature, concentration, stirring, impurities *etc.* As a well-known example, the complex $[Fe(Htrz)_2(trz)]BF_4$ (trz = 1,2,4-triazole) can be isolated into two polymorphs depending on the solvent used for the crystallization (water/ethanol mixture or pure methanol).[16] One polymorph displays high temperature hysteretic transitions centered at 365 K while the other shows the ST centered at 335 K. Either SCO or ferroelectric properties were detected for different polymorphs of a chiral Fe(II) complex $[FeL_3](BF_4)_2$ (L = (*S*)-1-phenyl-*N*-(1-butyl-imidazole-2-ylmethylene)ethylamine).[17] Many other Fe(II), Fe(III) and Co(II) SCO complexes were found in different polymorphic forms.[18–33]

In this paper we focus on the polymorphism effect in a molecular Fe(II) complex with *N*,*N*′-bis(5-bromopyridin-2-ylmethyl)ethane-1,2-diamine (L_{Br}) and dicyanamide (dca) ligands, $[FeL_{Br}(dca)_2]$, which can be selectively obtained in three diverse crystalline forms depending on the synthetic protocol and showing distinct SCO properties.

Results and discussion

Polymorphism in $[FeL_{Br}(dca)_2]$

It is not a facile task to obtain the desired polymorph since the free energy difference between polymorphs is usually quite small (a few kJ mol^{-1}) and mostly depends on the entropic contribution to the free energy. In contrast to many previously obtained SCO polymorphic mixtures, this is one of the not many cases when any of these three polymorphs can be selectively prepared in a pure form by a delicate control over the reaction temperature. The polycrystalline powder of the α-form is obtained by fast precipitation from the reaction of $Fe(ClO_4)_2{\cdot}6H_2O$, L_{Br} and sodium dicyanamide in MeCN in an ice bath. The polycrystalline powder of the β-form would be obtained instead if the same reaction was carried out at room temperature. Recrystallization of the powder from hot MeCN and then keeping the solution at 4 °C gives crystals of the γ-form as a pure phase. If this solution is kept at a lower temperature (−5 °C), a mixture of α and β (major product) crystals is formed instead. Hence the α-form is considered to be a kinetic product while the γ-form is a thermodynamic product. All three polymorphs have very different crystal morphologies that can be easily distinguished using a microscope (Fig. 1). Their phase purity was checked by comparing the powder X-ray diffraction patterns to those simulated from the single-crystal X-ray structural data (Fig. S1–S3, ESI†).

Magnetic properties of α–γ polymorphs

Magnetic susceptibility data were recorded on polycrystalline samples between 10 and 300 K in both the cooling and heating modes. The results are shown in Fig. 2 in the form of $\chi_M T$ *versus* T plots (where χ_M is the molar magnetic susceptibility and T is temperature). The $\chi_M T$ product of the α-form is 3.4 cm^3 mol^{-1} K at 300 K and decreases slightly to 3.3 cm^3 mol^{-1} K at 142 K at a cooling rate of 2 K min^{-1}, indicating that the Fe^{II} ions are in the HS state. Below 142 K, an abrupt decrease of the $\chi_M T$ value was observed. The value of 0.1 cm^3 mol^{-1} K at 114 K corresponds to a complete spin conversion (less than 3% of the residual HS Fe(II) centers). The measurement performed in the subsequent heating mode revealed a thermal hysteresis evidencing a first order transition. A theoretical simulation of the SCO in the α-form is given in the ESI† (Fig. S4). The thermal hysteresis width is dependent on the temperature scan rate (Fig. 3 and Fig. S5, ESI†). At 2 K min^{-1} scan rate, the transition temperatures (for which 50% of the spins are converted) are $T_{1/2}\downarrow$ = 129.0 K in the cooling mode and $T_{1/2}\uparrow$ = 137.3 K in the heating mode, resulting in a 8.3 K wide hysteresis. The width of hysteresis is reduced to 4.7 K at 0.5 K min^{-1} and 2.8 K at a 0.2 K min^{-1} scan rate.

The $\chi_M T$ value of the β-form is 3.3 cm^3 mol^{-1} K at 300 K and decreases slightly to 3.1 cm^3 mol^{-1} K at 159 K, indicating that the Fe^{II} ions are in the HS state. Upon cooling, the $\chi_M T$ value

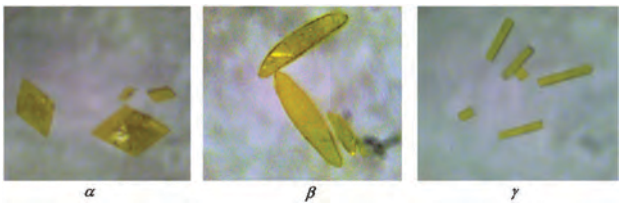

Fig. 1 Photographs of single crystals of the three polymorphs isolated for $[FeL_{Br}(dca)_2]$.

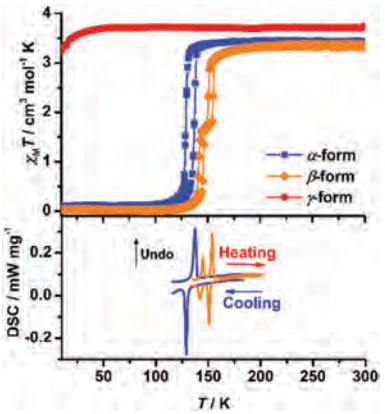

Fig. 2 Top: Temperature dependence of the $\chi_M T$ product at 2 K min^{-1} for the three polymorphs. Down: Differential scanning calorimetry (DSC) for the α and β forms.

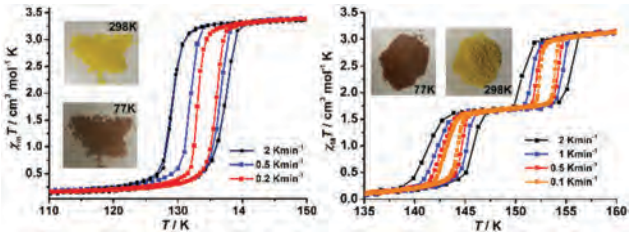

Fig. 3 Scan rate dependent hysteresis loops of $\chi_M T$–T curves for α (left) and β (right) forms. The insets are photos of the corresponding polymorphs at 298 and 77 K, showing their ST associated thermochromism.

drops sharply to 1.7 cm^3 mol^{-1} K at 147 K, corresponding to a half spin transition of the metal ions. A second abrupt decrease of $\chi_M T$ was observed below 142 K to an almost zero value below 125 K, corresponding to the ST of the remaining metal ions. The values of the transition temperatures in both the cooling and heating modes are dependent on the temperature scan rate (right part of Fig. 3), giving a linear decrease of the width of hysteresis (Fig. S6, ESI†) from *ca.* 4.5 K at 2 K min^{-1} to 0.7 K at 0.2 K min^{-1} scan rate, for both steps.

The $\chi_M T$ value of the γ-form at 300 K is 3.7 cm^3 mol^{-1} K, lying in the range typically observed for Fe(II) ion in the HS state. This value remains relatively constant until 50 K and a decrease observed below 50 K comes from the zero field splitting.

Both the α and β polymorphs show a striking color change associated with the spin transition, from bright yellow at room temperature to dark red at liquid nitrogen temperature (see the insets in Fig. 3). The first order phase transition associated with the SCO process was confirmed by differential scanning calorimetry (DSC; Fig. 2). One set of exothermic/endothermic peaks related to the one-step ST was found for the α-form. The average ΔH and ΔS values were estimated to be 5.3 kJ mol^{-1} and 39.8 J K^{-1} mol^{-1}. In comparison, two peaks corresponding to the two-step transition were observed for the β-form at $T_{1/2}\downarrow(1)$ = 150.7 K and $T_{1/2}\downarrow(2)$ = 141.9 K in the cooling mode and at $T_{1/2}\uparrow(1)$ = 153.6 K and $T_{1/2}\uparrow(2)$ = 144.8 K in the heating mode, in good agreement with the magnetic measurements. The corresponding average ΔH and ΔS values were estimated to be 2.8/1.5 kJ mol^{-1} and 18.5/10.7 J K^{-1} mol^{-1} for the first/second step.

Crystal structures of α–γ polymorphs in their HS state

The crystal structures of the three polymorphs were firstly determined in their HS state at 298 K. The crystallographic data and refinement parameters are listed in Tables 1 and 2. They crystallize in three different space groups: the orthorhombic space group *Pcan* for the α-form, the monoclinic space group $P2_1/n$ for the β-form and the monoclinic space group $P2/n$ for the γ-form. They all consist of $[FeL_{Br}(dca)_2]$ neutral molecules without interstitial solvent molecules. As shown in Fig. 4, the tetradentate ligand wraps an iron(II) metal ion in a *cis*-α conformation, leaving two *cis* positions for the dca co-ligands. As imposed by the tetradentate ligand, the Fe(II) center can adopt either Δ or Λ chirality thus leading to racemic compounds. In the α and γ polymorphs, the Fe(II) ion is centered on a 2-fold axis and the asymmetric unit comprises half of a complex while in the β-form the entire complex is present in the asymmetric unit. The most significant difference in their molecular arrangements are manifested by the configuration of the dca co-ligands. Firstly, the dangling cyanide group points in different directions, as seen by the different distances between the two dangling N atoms (~9.7, 4.8 and 9.2 Å in the α–γ forms, respectively) and the different torsion angles between the two dangling CN groups (~146, 63 and 34° in α–γ forms, respectively); secondly, the $Fe–N_{dca}–C_{dca}$ angle deviates from the ideal 180° to different degrees (~159° in α, 143 and 157° in β and 161° in γ). Differences in the first coordination sphere of the metal center are also observed: firstly, the average Fe–N bond lengths in the γ-form (2.18 Å at 123 K) is obviously longer than those in the α and β forms (2.13 Å at 298 K); secondly, the FeN_6 octahedron is distorted to different extents in the three polymorphs, as indicated by the octahedral distortion parameters Σ and Θ in Table 2. (Σ is the sum of deviations from 90° of the 12 *cis* N–Fe–N angles; Θ is the sum of the deviations from 60° of the 24 possible octahedron twist angles.[34,35])

In all three polymorphs, each $[FeL_{Br}(dca)_2]$ complex is involved in a large variety of intermolecular interactions with many neighbouring complexes (see Fig. S7, ESI†). In particular the dca ligands exhibit multiple interactions, including NH···dca hydrogen bonds, Br···dca halogen bonds, and C–H···dca and C···dca short contacts, providing 3D connectivity in the lattices. Among these interactions, the hydrogen bonds between the dangling CN of dca ligands and the H atoms of amine groups

Table 1 Crystal data and refinement details for α–γ polymorphs

	α-Polymorph		β-Polymorph			γ-Polymorph	
Temperature/K	298	123	298	146	123	298	123
Crystal system	Orthorhombic	Orthorhombic	Monoclinic	Monoclinic	Monoclinic	Monoclinic	Monoclinic
Space group	*Pcan*	$P22_12_1$	$P2_1/n$	$P2_1$	$P2_1/n$	$P2/n$	$P2/n$
a/Å	8.707(3)	8.8256(8)	8.7376(19)	8.8548(5)	8.7407(9)	7.3713(8)	7.3304(5)
b/Å	14.128(4)	13.4735(12)	12.499(2)	12.5141(7)	12.4108(13)	7.8546(7)	7.7934(5)
c/Å	16.875(5)	17.2070(16)	19.217(4)	19.2074(11)	19.0055(19)	18.746(2)	18.5912(14)
β/°	90	90	93.267(8)	93.534(2)	94.212(4)	97.334(4)	97.229(3)
Volume/Å^3	2075(1)	2046.1(3)	2095.4(7)	2124.3(2)	2056.1(4)	1076.64(19)	1053.65(13)
Z	4	4	4	2	4	2	2
ρ_{calc}/mg mm^{-3}	1.882	1.909	1.864	1.839	1.900	1.814	1.854
μ/mm^{-1}	4.606	4.673	4.563	4.501	4.650	4.440	4.537
F(000)	1160.0	1160.0	1160.0	1160.0	1160.0	580.0	580.0
Reflections collected	9618	118 489	16 896	7464	15 769	5923	7090
Flack	—	0.54(3)[b]	—	0.19(2)[b]	—	—	
R_{int}	0.0701	0.0700	0.0802	0.0696	0.0751	0.0679	0.0696
GOF on F^2	1.106	1.018	1.148	1.033	1.055	1.121	1.074
R_1, wR_2[a] [$I \geq 2\sigma(I)$]	0.0439, 0.0994	0.0345, 0.0601	0.0605, 0.1091	0.0572, 0.0854	0.0403, 0.0660	0.0579, 0.0925	0.0401, 0.0592
R_1, wR_2[a] [all data]	0.0849, 0.1163	0.0641, 0.0687	0.1169, 0.1347	0.0926, 0.0941	0.0761, 0.0767	0.0925, 0.1017	0.0638, 0.0653

[a] $R_1 = \sum||F_o| - |F_c||/\sum|F_o|$. w$R_2 = (\sum[w(F_o^2 - F_c^2)^2]/\sum[w(F_o^2)^2])^{1/2}$. [b] Structure was refined as an inversion twin.

Table 2 Selected bond lengths and structural parameters for α–γ polymorphs

	α-Polymorph			β-Polymorph				γ-Polymorph	
T/K	298	123		298	146		123	298	123
Spin state	HS	LS	LS	HS	HS	LS	LS	HS	HS
Fe–N_{av}/Å	2.13	1.97	1.97	2.13	2.15	1.98	1.97	2.18	2.18
Fe–N_{dca}/Å	2.068(7)	1.956(8)	1.958(8)	2.067(8)	2.087(11)	1.951(11)	1.951(4)	2.110(5)	2.106(4)
				2.076(8)	2.100(12)	1.959(10)	1.952(4)		
Fe–N_{py}/Å	2.181(6)	1.969(7)	1.963(7)	2.154(7)	2.180(9)	1.981(10)	1.960(4)	2.226(4)	2.216(3)
				2.165(7)	2.172(10)	1.986(10)	1.964(4)		
Fe–N_{amine}/Å	2.150(6)	1.997(8)	1.992(8)	2.175(7)	2.180(10)	2.020(10)	1.992(4)	2.226(5)	2.224(3)
				2.184(7)	2.189(9)	2.029(10)	1.997(4)		
Fe–N–C_{dca}/°	159.0(7)	165.5(7)	165.3(7)	143.3(8)–157.1(8)	142.4(11)–160.8(11)	156.9(11)–164.4(11)	154.5(4)–165.1(4)	161.9(5)	161.0(3)
N_{dca}–Fe–N_{dca}/°	94.3(3)	89.2(4)	90.1(5)	93.4(3)	93.6(4)	88.1(4)	88.15(18)	102.2(3)	102.5(2)
cis N–Fe–N/°	74.4(2)–99.3(2)	80.9(3)–96.6(3)	82.9(3)–93.8(3)	76.6(3)–96.3(3)	76.2(4)–98.3(4)	81.8(4)–94.8(4)	83.9(2)–95.3(2)	74.1(1)–102.2(3)	74.4(1)–102.5(2)
trans N–Fe–N/°	165.7(2)–172.0(3)	172.8(3)–176.7(5)	165.8(1)–172.7(1)	166.3(3)–168.1(3)	165.1(4)–170.1(4)	170.9(4)–177.0(4)	171.7(1)–177.4(1)	164.1(2)–168.8(3)	163.8(1)–169.1(2)
Σ_{Fe}/°	81.7(9)	47.8(16)	35.1(16)	73.1(9)	76.4(13)	43.6(17)	40.1(6)	82.6(7)	81.8(6)
Θ	236(2)	149(3)	92(3)	173(2)	197(3)	113(3)	104.2(13)	221.6(17)	217.5(12)

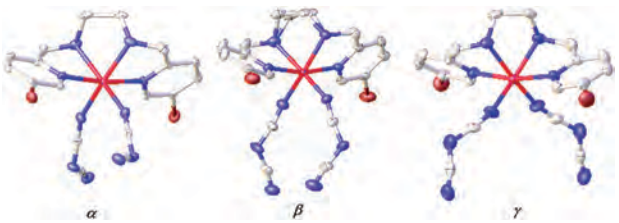

Fig. 4 View of the molecular structures of the HS Fe(II) complex in the α (left), β (middle) and γ (right) polymorphs at 298 K. Hydrogen atoms are deleted for clarity. Thermal ellipsoids are presented at 50% probability. Color code: Fe, red; C, grey; Br, brown; N, blue.

are much stronger and appear to play a dominant role in the crystal packing of these compounds (Tables S1–S3, ESI†). In the case of the α and β forms, pairs of NH···NC hydrogen bonds between adjacent complexes (of alternating upward and downward orientations) give rise to strongly coupled chains of complexes along the *c* and *b* axis, respectively (Fig. 5a and b). The strength of the interactions is comparable in the α and β forms as indicated by the similar distances between N atoms (~3 Å) and the similar N–H···N angles (155–171°). In contrast, those NH···NC hydrogen bonds in the γ-form connect the complexes into 2D layers that are parallel to the *ab* plane (Fig. 5c). A larger N···N distance around 3.2 Å and a smaller N–H···N angle around 134° in the γ-form suggest considerably weaker hydrogen bonding. In addition, molecules in the α-form are aligned along the *a* axis and CH···N hydrogen bonds (C···N ~ 3.5 Å, C–H···N ~ 160°) are observed between the dca and ethylene groups (Fig. S8, ESI†). In the γ-form molecules are also packed in a linear array along the *b* axis. While different from the α-form, $NHCH_2CH_2NH$ backbones are embedded by two dca arms and form CH···C short contacts (H···C ~ 2.6 Å) instead (Fig. 5c). In the β-form the two dca arms are too close to embrace a $NHCH_2CH_2NH$ backbone. Alternatively, C–H(methylene)···C(pyridine) short interactions (H···C ~ 2.6 Å) are prevalent in the β-form, giving a 1D linear chain along the *a* axis (Fig. S9, ESI†). Besides, Br···NC halogen

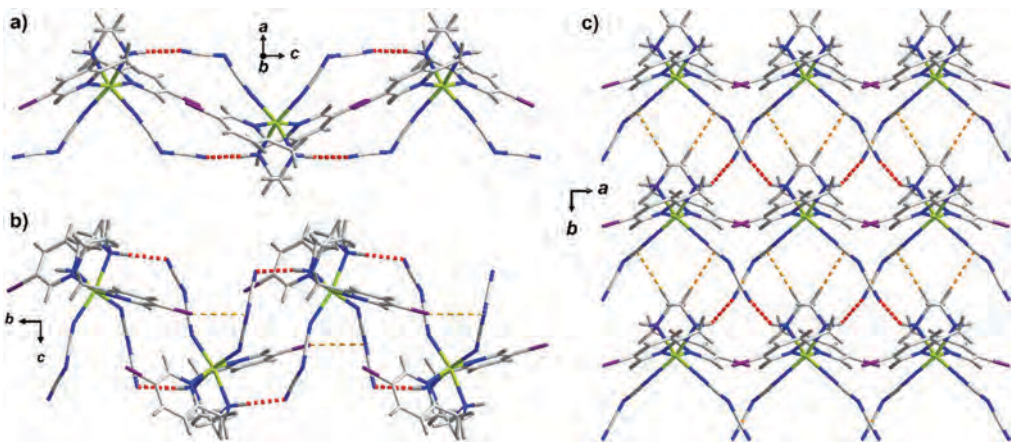

Fig. 5 Chains in α (a), β (b) and 2D layer in γ-form (c) linked by hydrogen bonds between the CN of dca ligands and H atoms of amine groups (red dotted lines). Halogen bonds in β-form and C–H(ethylene)···C(dca) interactions in the γ-form are also shown with orange dotted lines. Color code: C, light grey; H, grey; Fe, green; N, blue; Br, violet.

bonds (Br···N ~ 3.2 Å, C–Br···N ~ 157°) are also found along the hydrogen bonded chains (Fig. 5b).

Crystal structures of the α and β forms in different spin states

The α-form shows the symmetry reduction associated with spin transition. The space group changes in $P22_12_1$ at 123 K and two distinct crystallography independent Fe(II) both sitting on the 2-fold axis are observed (Fig. S10, ESI†). The Fe1 site adopts an Λ chirality while the Fe2 site adopts Δ chirality. The Fe–N bond lengths for both sites (average 1.97 Å, Table 2) indicate they are in LS states at this temperature, in good agreement with magnetic study.

Overlay of the molecular structures at 298 and 123 K (see the left of Fig. 6) shows a significant rearrangement of the molecular structure. The dca co-ligands are flexible and provide a less distorted coordination environment in the LS state. The *cis* N_{dca}–Fe–N_{dca} angles are closer to 90° (~94° at 298 K and 89/90° at 123 K) and the Fe–N_{dca}–C_{dca} angles deviate less from the ideal 180° (~159° at 298 K and ~165° at 123 K). Notably, a flip of the conformation of the ethylene bridge in the tetradentate ligand around Fe2 site was observed. Such flipping is probably driven by the strong NH···NC hydrogen bonds to maintain their close contacts, which compensates for the movement of dca ligands. Hence an alternative running of Fe1 and Fe2 sites was formed along the chain linked by the NH···NC hydrogen bonds (Fig. 7). As indicated by the smaller Σ and Θ values at 123 K (see Table 2), the Fe(II) ions have more regular coordination geometries in the LS state.

Even though the symmetry breaks at 123 K, the crystal packing in the two spin phases are quite comparable. It should be noted that the α-form shows a thermal expansion in the *b* axis (4.6%) and an unusual negative thermal expansion in the *a* (−1.4%) and *c* (−2.0%) axes, resulting in a total volume decrease of about 1.4% from the HS to the LS phase. Superimposed *ab* and *ac* sub-lattices of the LS and HS phases are shown in Fig. S11 (ESI†). The Fe sites along the *b* axis move closer upon transition to the LS state, attributed greatly to the flip of the ethylene bridge at the Fe2 site. In contrast in the *a* and *c* directions the Fe centers do not shift obviously upon ST. Various supramolecular interactions become ~0.1 Å stronger upon transition to the LS phase. The NH···NC hydrogen bonds are comparable in the two phases with the N···N distance less than 3 Å. As analysed above this is a balance between the movement of the dca ligands and the flip of the ethylene group.

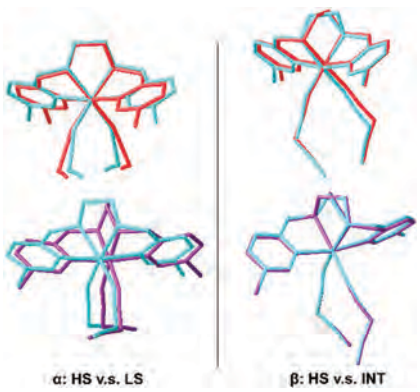

Fig. 6 Overlay of the molecular structures of the Fe(II) complexes in different spin phases. Left: α-Form in the HS phase (blue) and LS phase (Fe1 site in red and Fe2 site in purple). Right: β-Form in the HS phase (blue) and INT phase (HS site in purple and LS site in red).

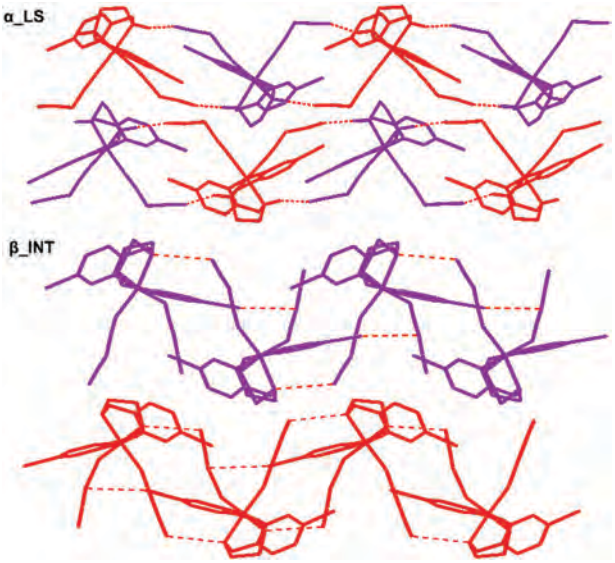

Fig. 7 Propagation of Fe sites along the NH···NC supramolecular chains in the LS phase of the α-form (top, Fe1 site in red and Fe2 site in purple) and in the INT phase of the β-form (bottom, HS site in purple and LS site in red).

The β-form shows a re-entrant symmetry change associated with the two-step spin transition. At 123 K (LS phase) it crystallizes in the same space group $P2_1/n$ as the HS phase while at 146 K (intermediate phase, *i.e.* INT phase) the monoclinic space group $P2_1$ was found. In the LS phase, there is a unique Fe(II) molecule in the LS state, with an average Fe–N bond length of ~1.97 Å. In the INT phase, there are two independent Fe(II) molecules in the asymmetric unit (see Fig. S12, ESI†) that are in different spin states (average Fe1–N ~ 2.15 Å; Fe2–N ~ 1.98 Å) and opposite chirality (Fe1, Δ chirality; Fe2, Λ chirality). The LS site has a more regular octahedral geometry than the HS site as indicated by the Σ and Θ parameters (Table 2). The ethylene group of the tetradentate ligand is disordered over two positions for the HS site in both the HS and INT phases while it is ordered for the LS sites in both the LS and INT phases. As seen by the overlay of molecular structures in different spin phases in the right of Fig. 6 and Fig. S13 (ESI†), the change is not as significant as in the α-polymorph. The molecules in different spin states (*i.e.* Fe2 in INT phase *vs.* Fe1 in the HS phase and Fe1 in INT phase *vs.* Fe1 in the LS phase) show a slight movement of the dca co-ligands and an order/disorder of the tetradentate ligand. The *cis* N_{dca}–Fe–N_{dca} angles decrease from 93° in HS state to 88° in LS state. Those in the same spin state (*i.e.* Fe1 in INT phase *vs.* Fe1 in HS phase and Fe2 in INT phase *vs.* Fe1 in LS phase) are almost superimposed.

The crystal packing of the β-form remains similar in the three phases. The supramolecular interactions are slightly increased upon transition to the LS phase. The strongest NH···NC and C–H(methylene)···C(pyridine) interactions link the homo-spin

Fe complexes into a 2D layer parallel to the *ab* plane. HS and LS supramolecular layers run alternatively along the *c* axis.

The crystallographic data of γ-form at 123 K confirm the HS state of the Fe complexes (average Fe–N bond length ~2.18 Å, see Tables 1 and 2 for details), in good agreement with the magnetic results. The structures at 123 and 298 K are well superimposable.

Discussion of the magnetic property in relation with the molecular and crystal structures

The report of three new complexes here is a continuing work of our group in studying the $[FeL(NCX)_2]$ family, where L is a pyridyl-diamine based tetradentate ligand and X is S/Se/BH_3.[25,36,37] dca is for the first time exploited and turns out to be also an appropriate co-ligand to construct appealing Fe(II) SCO materials in combination with such a tetradentate ligand. The terminal NCN of dca ligands have the potential to exhibits multiple short contacts and are helpful in enhancing the synergy of the SCO. So far 9 structures derived from this family have been isolated: 6 of them show spin-crossover properties with $T_{1/2}$ between 100 and 400 K, with 5 of which being of the first order nature. The remaining three are HS over all temperatures. This family shows a particular structural diversity in the solid state, crystallized in several different space groups with different molecular arrangements and crystal packings. Particularly in the present $[FeL_{Br}(dca)_2]$ derivative three polymorphs have been delicately separated. Comparison of these structures show that the monodentate co-ligands contributes most to the structural modifications since they can flexibly adopt different coordination orientations. Particularly for the dca co-ligand with a dangling cyanide group, additional variabilities arises from the uncoordinated cyanide since it could point toward different positions. For the previously reported analogues the geometry of tetradentate ligands is rather consistent due to the geometrical restriction imposed in the chelating mode. In the present study the flip and order–disorder of the ethylene group upon ST observed in α and β polymorphs show also the capacity of local adjustment in the tetradentate ligand. Such large rearrangement of the molecular structures is likely to contribute to the sharp switching between the HS and LS spin states.

In view of the crystal packing, different organizations between molecules and different sets of supramolecular interactions are observed for this family. Nevertheless, multiple intermolecular interactions between the co-ligands and the tetradentate ligands are present in all cases. Weak interactions are crucial for defining the SCO differences in polymorphic systems. Moreover, the ligand field on metallic centers is highly sensitive to the lattice. For example, Ueno *et al.* explained a difference in the SCO properties of two polymorphic crystals by the different assembly coming from the NH···Cl hydrogen bonding.[38] Weak interactions with solvent are responsible for the polymorphism in one complex described by Salitros *et al.*[15] The terminal CN of dca ligands contribute abundant short contacts in the three polymorphic forms of $[FeL_{Br}(dca)_2]$ compounds. The strong NH···NC hydrogen bonds together with the Br···dca, C–H···dca, C···dca and C···C short contacts are supposed to play an important role in propagating communications between switching centers and tend to give SCO systems of high cooperativity.

As shown in Fig. 5c, molecules in the γ-form pack into a regular layer linked by NH···NC hydrogen bonds. In contrast to the other two polymorphs, the *cis* N_{dca}–Fe–N_{dca} angle (102°) strongly deviates from the ideal 90°. The two dca arms enclose an ethylene group and form strong C–H···C interactions. It is expected if a HS to LS transition happened, the *cis* N_{NCX}–Fe–N_{NCX} angle would significantly decrease and would get closer to 90°. This is supported by all our previous observations for SCO complexes from this family. Particularly, in $[Fe^{2Me}L_{pz}(NCBH_3)_2]$ ($^{2Me}L_{pz}$ = *N*,*N*′-dimethyl-*N*,*N*′-bis((pyrazin-2-yl)methyl)-1,2-ethanediamine), the N_{NCBH_3}–Fe–N_{NCBH_3} angle decreases from 106° in the HS phase to 97° in the LS phase.[37] In the γ-form such an adjustment is disfavoured as one can imagine that the approach of the two dca arms would weaken the hydrogen bonding and would be sterically hindered by the embedded ethylene group.

Mössbauer studies of α and β polymorphs

Mössbauer spectra of the α-form were recorded in the 180–100 K temperature range in the cooling mode (Fig. 8). All obtained hyperfine parameters are summarized in Table 3. A 179.8 K spectrum shows the presence of the HS Fe(II) doublet (δ = 0.95 mm s^{-1}, ΔE_Q = 1.12 mm s^{-1}). Upon cooling, a new doublet corresponding to Fe(II) LS emerges (at 134.4 K δ = 0.52 mm s^{-1}, ΔE_Q = 0.13 mm s^{-1}). The content of the LS form grows upon cooling: 15% (134.4 K), 56% (133.9 K) and 81% (132.9 K). At 100.5 K the LS content constitutes 100%. This confirms that the spin transition occurs between pure HS and LS forms.

Mössbauer spectra of the β-form were recorded within the 233–100 K temperature range in the cooling mode (Fig. 9 and Fig. S15, ESI†). All obtained hyperfine parameters are summarized in Table 4. A Mössbauer spectrum at 233.0 K shows one HS Fe(II) doublet (δ = 0.97 mm s^{-1}, ΔE_Q = 1.95 mm s^{-1}) and a minor LS Fe(II) contribution of 2.6% (δ = 0.41 mm s^{-1}). Upon cooling to 180.1 K the LS Fe(II) contribution gives a small rise to 4.8%, and the HS Fe(II) content drops consequently.

A 152.1 K Mössbauer spectrum shows a considerably different image. One can see the appearance of two HS doublets on the

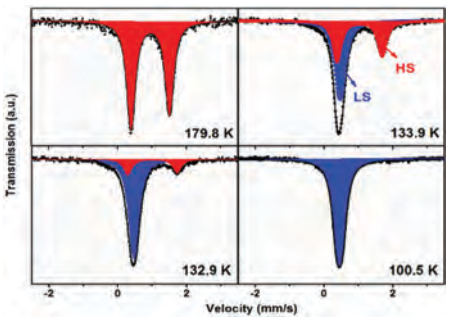

Fig. 8 Selected ^{57}Fe Mössbauer spectra of the α-form recorded in the 180–100 K temperature range. The spectra were deconvoluted into peaks from the HS (red) and LS (blue) sites.

Table 3 Mössbauer hyperfine parameters of the α-form at different temperatures

	T/K	179.8	134.4	133.9	132.9	100.5
HS	δ/mm s^{-1}	0.954(3)	1.0483(10)	1.037(3)	1.010(6)	—
	ΔE_Q/mm s^{-1}	1.118(5)	1.318(2)	1.313(5)	1.436(12)	—
	Linewidth/mm s^{-1}	0.145(4)	0.145[a]	0.145[a]	0.145[a]	—
	Fraction/%	100	84.6(6)	43.6(7)	19.0(8)	0
LS	δ/mm s^{-1}	—	0.520(6)	0.471(2)	0.478(14)	0.451(11)
	ΔE_Q/mm s^{-1}	—	0.132[a]	0.132[a]	0.132[a]	0.132(5)
	Linewidth/mm s^{-1}	—	0.153[a]	0.153[a]	0.153[a]	0.153(3)
	Fraction/%	0	15.4(4)	56.4(6)	81.0(6)	100

[a] This parameter was fixed during the fit.

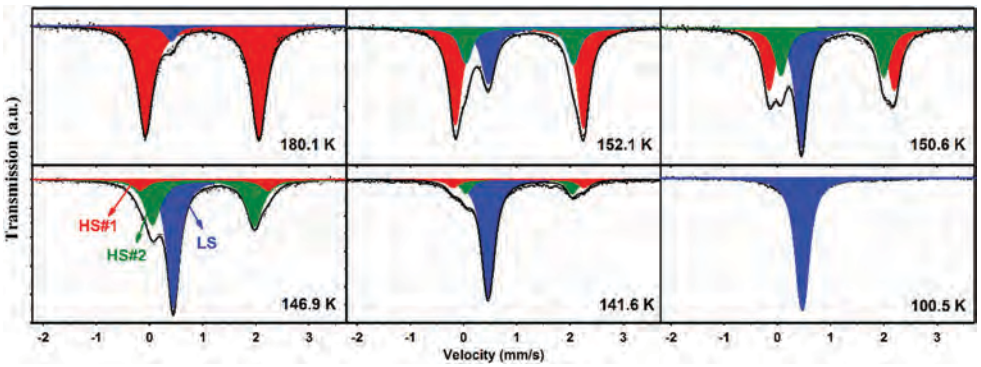

Fig. 9 ^{57}Fe Mössbauer spectra of the β-form recorded in the 180–100 K temperature range. The spectra were deconvoluted into subspectra corresponding to HS#1 (red), HS#2 (green) and LS (blue) sites.

Table 4 Mössbauer hyperfine parameters of the β-form at different temperatures within the 100–233 K region. The contributions of HS#1 fraction, HS#2 fraction and LS fraction are given

T/K		233.0	180.1	152.1	150.6	146.9	141.6	100.5
HS#1	δ/mm s^{-1}	0.968(3)	0.990(2)	1.0505(13)	1.023(3)	1.004(16)	1.037(9)	—
	ΔE_Q/mm s^{-1}	1.953(6)	2.131(5)	2.409(4)	2.352(7)	2.35(5)	2.46(2)	—
	Linewidth/mm s^{-1}	0.172(5)	0.174(4)	0.136[a]	0.136[a]	0.172[a]	0.136[a]	—
	Fraction/%	97.4(2)	95.2(17)	59.7(9)	36.1(9)	10.9(2)	9.4(7)	—
HS#2	δ/mm s^{-1}	—	—	1.054(4)	1.036(4)	1.011(4)	1.044(5)	—
	ΔE_Q/mm s^{-1}	—	—	2.017(11)	1.930(10)	1.909(15)	1.992(13)	—
	Linewidth/mm s^{-1}	—	—	0.136[a]	0.136[a]	0.172[a]	0.136[a]	—
	Fraction/%	—	—	21.9(9)	28.1(9)	41.3(2)	17.2(7)	—
LS#1	δ/mm s^{-1}	0.411[a]	0.41(2)	0.47(3)	0.4551(19)	0.4479(18)	0.4620(8)	0.4779(7)
	ΔE_Q/mm s^{-1}	—	—	—	—	—	0.091(5)	0.091(5)
	Linewidth/mm s^{-1}	0.127[a]	0.127[a]	0.149(5)	0.139(3)	0.136(3)	0.124(2)	0.127(2)
	Fraction/%	2.6(8)	4.8(6)	18.5(5)	35.8(6)	47.8(8)	73.4(6)	100

[a] This parameter was fixed during the fit.

spectra (marked as HS#1 and HS#2). These two HS forms are present at the quantities of 60 and 22% for the HS#1 (δ = 1.05 mm s^{-1}, ΔE_Q = 2.41 mm s^{-1}) and HS#2 (δ = 1.05 mm s^{-1}, ΔE_Q = 2.02 mm s^{-1}), respectively. The LS Fe(II) peak at this temperature has a contribution of 18%. As the quantities of HS#2 and LS are almost the same, we can suppose that all LS Fe(II) centers come from the intermediate HS–LS phase. On the other hand, this can be also interpreted as a complex superposition of the HS and LS centers in the intermediate phase that leads to different HS signals. However, there is no indication of that from the crystallographic data (Fe–N LS length is the same in LS and LS–HS phases, and the HS length is the same in the LS–HS and HS phases).

It is worth mentioning that at 233.0 and 180.1 K we probably also have two HS forms (see also the alternative fitting in Fig. S16 and Table S4, ESI†), however because of a small fraction the HS#2 cannot be correctly distinguished.

A 150.6 K Mössbauer spectrum looks similar to the previous one (152.1 K), however the content of all the Fe forms is different: that of the HS#1 is 36%, HS#2 is 28% and LS is 36%.

The content of LS Fe(II) at this temperature is higher compared to the HS#2. The contribution of different LS centres cannot be considered separately since their doublets have practically the same isomer shifts and quadrupole splittings (see the alternative fitting in Fig. S17 and Table S4, ESI†).

The same co-existence of spin forms is observed at 146.9 K. The transition temperatures corroborate well between the magnetic and Mössbauer experiments (even though some small difference is due to the different timescales of the two techniques). The 146.9 K spectrum corresponds to the plateau of the spin transition curve (48% of the LS fraction from the Mössbauer spectra). This allowed refining the crystal structure of the HS–LS phase, since it makes a major contribution near this temperature.

At 141.6 K the content of the HS drops, and at 100.5 K only the LS signal is observed.

There are different possible explanations for this unusual co-existence of spin forms. The phase coexistence would make sense if the content of the HS phase drops and the content of the LS phase increases on cooling, while the content of the HS–LS phase changes inhomogeneously and reaches the maximum around the plateau. However, a deep additional analysis is necessary to make a definitive conclusion on the nature of this unusual phenomenon.

Conclusions

We have shown that a new Fe(II) complex, $[FeL_{Br}(dca)_2]$, can be obtained in three polymorphic forms displaying completely different magnetic behavior. The α-form undergoes a one-step spin transition around 134 K with a 8.3 K wide hysteresis (at a temperature scan rate of 2 K min^{-1}). The β-form displays a two-step spin transition ($T_{1/2}$ = 153 and 144 K) and shows a 4.5 K wide hysteresis for each step (at 2 K min^{-1}). In contrast the γ-form is stabilized in its HS state over all temperature range. The structural diversity mainly arises from the flexible coordination geometry adopted by the monodentate dca ligand. Although the three polymorphic forms have clearly different molecular arrangements and crystal packings, dense packing without interstitial solvents and abundant supramolecular interactions between the tetradentate and dca ligands are observed among all of them. Such a dense network is supposed to create strong elastic interactions between the Fe(II) centers and favours the occurrence of a first order phase transition. Particularly, the NH···NC hydrogen bonds are found to play a crucial role in discriminating between different magnetic behaviours in the three polymorphs. The hydrogen bonds in γ-form link molecules into a 2D network and inhibit the occurrence of spin transition. Symmetry breaking observed for the α-form is rare among complexes showing one-step SCO. A single Fe(II) site in the HS state converts to two crystallographically distinct Fe(II) sites in the LS state, driven by the NH···NC hydrogen bonds. The two-step transition for the β-form is related to a re-entrant symmetry change, which offers an ordered HS–LS arrangement in the range of the plateau. However the Mössbauer spectroscopy reveals the unusual composition of the HS, HS–LS and LS phases during the two-step SCO, indicating a complicated evolution of the spin phase – rather than a simple transformation from classic HS to HS–LS and then from the HS–LS to the LS phase.

Experimental section

All reagents obtained from commercial sources were used without further purification. Safety Note: perchlorate salts are potentially explosive, and caution should be taken when dealing with such materials.

Synthetic procedures

The tetradentate ligand *N*,*N*′-bis[(5-bromo-2-pyridyl)methyl]ethane-1,2-diamine (L_{Br}) was prepared according to the literature.[39] The syntheses of the complexes were carried out under an N_2 atmosphere.

Selective synthesis of α-form (polycrystalline powder)

To a 20 mL CH_3CN solution of $Fe(ClO_4)_2{\cdot}6H_2O$ (0.036 g, 0.1 mmol) in an ice bath was added 0.040 g of L_{Br} and 0.019 g of sodium dicyanamide (2 mmol). The α-form precipitates as a yellow powder immediately and was collected by filtration after an hour and washed with mother liquid. The yield is 58%.

Selective synthesis of β-form (polycrystalline powder)

The β-polymorph was prepared similarly to the α-form except that the reaction was carried out at room temperature. The polycrystalline of pure β-form (yellow powder) was collected by filtration and washed with MeOH. The yield is 55%.

Selective synthesis of γ-form (single crystals)

Recrystallization of the precipitates of the α- or β-form in hot MeCN and then kept at 4 °C give prismatic crystals of the pure γ-form in 38% yield.

Synthesis of single crystals of the α- and β-forms

Single crystals suitable for X-ray determination of the α- and β-forms were prepared similarly to the γ-form except that the solution was kept at −5 °C. Block yellow crystals of β-form was obtained as a major product while needle yellow crystals of α-form appeared as a by-product. They could be easily distinguished and separated under the microscope.

Elemental analyses

Calcd: C, 36.76; H, 2.74; N, 23.82. Found for the α-form: C, 36.57; H, 2.80; N, 24.50; found for the β-form: C, 36.68; H, 2.79; N, 23.73; found for the γ-form: C, 36.76; H, 2.70; N, 23.87.

IR spectra. The three phases show practically the same IR absorptions around the same wavenumbers (diamond ATR, cm^{-1}): 3231(N–H), 2276, 2212, 2143 (vs, C≡N), 1642, 1459, 1353, 1229, 1133, 1096, 1022, 940, 848, 816, 646.

Physical characterization

Magnetic susceptibility measurements were recorded with a Quantum Design PPMS-9, operating with an applied field of 0.1 T at temperatures from 10 to 300 K at rates between 0.1–2 K min^{-1}. Elemental analyses were performed using an Elementar Vario EL Elemental Analyser. IR spectra were recorded by the attenuated-total-reflectance (ATR) technique in the range 4000–650 cm^{-1} using a Perkin-Elmer Spectrum. DSC measurement was performed on a METTLER TOLEDO DSC1 instrument under a nitrogen atmosphere at a scan rate of 5 K min^{-1} in both the heating and cooling modes. PXRD patterns were recorded on a D8 ADVANCE X-ray diffractometer (Kα radiation, λ = 0.154056 nm). The ^{57}Fe Mössbauer spectra were measured in a transmission geometry employing a Mössbauer spectrometer operating in a constant acceleration mode and equipped with a ^{57}Co(Rh) source. The isomer shift values refer to metallic α-Fe at room temperature. Elemental analyses were performed using an Elementar Vario EL elemental analyser. The IR spectra were recorded using KBr discs in the range 4000–500 cm^{-1} with a Perkin-Elmer Spectrum.

Single crystal X-ray diffraction

Single-crystal X-ray data were collected on a Bruker D8 Quest diffractometer using graphite monochromated Mo-Kα radiation (λ = 0.71073 Å). A multi-scan absorption correction was performed (SADABS, Bruker, 2016). The structures were solved using the direct method (SHELXS) and refined by full-matrix least-squares on F^2 using SHELXL[40] under the graphical user interface of Olex2.[41] Non-hydrogen atoms were refined anisotropically. Hydrogen atoms were placed in calculated positions with C–H (aromatic) distances of 0.93 Å and C–H (methylene) distances of 0.97 Å. They were refined using idealized geometries (riding model) and assigned fixed isotropic displacement parameters ($1.2U_{eq}$(C or N)). The structures of the α-form were acquired in the HS (298 K) and in LS (123 K) phases. The HS phase structure was solved in the centrosymmetric *Pcan* space group. The LS phase structure was solved in a non-centrosymmetric $P22_12_1$ space group and refined as an inversion twin with BASF = 0.54(3). HS (298 K) and LS (123 K) crystal structures of the β-form were solved in the centrosymmetric $P2_1/n$ space group, while the HS–LS (146 K) phase structure was solved in the non-centrosymmetric $P2_1$ space group. The ADP of some C and N atoms and some C–C and C–N bond lengths were restrained. In the HS moieties (both in HS and HS–LS phases), ethylene bridges in the ligand were treated as disordered between two positions (0.68 : 0.32). The HS–LS structure of the β-form was refined as containing 19% of a racemic component. However, this may also be a contribution from the other phases present at this temperature in minor quantities and interpreted by the software as a racemic contribution. CCDC 1582828–1582833 and 1816546 contain the supplementary crystallographic data for this paper.†

Conflicts of interest

There are no conflicts to declare.

Acknowledgements

This work was supported by the National Natural Science Foundation of China (21401104), the Priority Academic Program Development of Jiangsu Higher Education Institutions and the Ministry of Education and Science of Ukraine (16BF037-03).

Notes and references

1 A. Saini, R. Chadha, A. Gupta, P. Singh, S. Bhandari, S. Khullar, S. Mandal and D. S. Jain, *Pharm. Dev. Technol.*, 2015, 1–8.
2 M. Haisa, S. Kashino, R. Kawai and H. Maeda, *Acta Crystallogr., Sect. B: Struct. Crystallogr. Cryst. Chem.*, 1976, **B32**, 1283–1285.
3 J. Kypr, I. Kejnovska, D. Renciuk and M. Vorlickova, *Nucleic Acids Res.*, 2009, **37**, 1713–1725.
4 M. Z. K. R. Seddon, *Crystal Engineering The Design and Application of Functional Solids*, Springer, Dordrecht, Netherlands, 1999.
5 M. A. Halcrow, *Spin-Crossover Materials Properties and Applications*, John Wiley & Sons, Ltd, Chichester, 2013.
6 P. Gütlich and H. A. Goodwin, *Spin Crossover in Transition Metal Compounds I*, 2004, pp. 1–47.
7 J. A. Real, A. B. Gaspar and M. C. Muñoz, *Dalton Trans.*, 2005, 2062–2079.
8 S. Rodríguez-Jiménez, H. L. C. Feltham and S. Brooker, *Angew. Chem., Int. Ed.*, 2016, **55**, 15067–15071.
9 T. Miyamachi, M. Gruber, V. Davesne, M. Bowen, S. Boukari, L. Joly, F. Scheurer, G. Rogez, T. K. Yamada, P. Ohresser, E. Beaurepaire and W. Wulfhekel, *Nat. Commun.*, 2012, **3**, 938.
10 J. Dugay, M. Aarts, M. Giménez-Marqués, T. Kozlova, H. W. Zandbergen, E. Coronado and H. S. J. van der Zant, *Nano Lett.*, 2017, **17**, 186–193.
11 M. Seredyuk, A. B. Gaspar, V. Ksenofontov, S. Reiman, Y. Galyametdinov, W. Haase, E. Rentschler and P. Gütlich, *Chem. Mater.*, 2006, **18**, 2513–2519.
12 J. Tao, R.-J. Wei, R.-B. Huang and L.-S. Zheng, *Chem. Soc. Rev.*, 2012, **41**, 703–737.
13 C. Bartual-Murgui, C. Codina, O. Roubeau and G. Aromí, *Chem. – Eur. J.*, 2016, **22**, 12767–12776.
14 W. Phonsri, C. G. Davies, G. N. L. Jameson, B. Moubaraki and K. S. Murray, *Chem. – Eur. J.*, 2016, **22**, 1322–1333.
15 I. Šalitroš, O. Fuhr and M. Ruben, *Materials*, 2016, **9**, 585.
16 K. Jonas, A. Jean-Paul, C. Renée, C. Epiphane, K. Olivier, J. G. Haasnoot, G. Françoise, J. Charlotte, A. Bousseksou, L. Jorge, V. François and G. V. Anne, *Chem. Mater.*, 1994, **6**, 1404–1412.
17 W.-K. Han, L.-F. Qin, C.-Y. Pang, C.-K. Cheng, W. Zhu, Z.-H. Li, Z. Li, X. Ren and Z.-G. Gu, *Dalton Trans.*, 2017, **46**, 8004–8008.
18 G. Agustí, C. Bartual, V. Martínez, F. J. Muñoz-Lara, A. B. Gaspar, M. C. Muñoz and J. A. Real, *New J. Chem.*, 2009, **33**, 1262.
19 M. B. Bushuev, V. A. Daletsky, D. P. Pishchur, Y. V. Gatilov, I. V. Korolkov, E. B. Nikolaenkova and V. P. Krivopalov, *Dalton Trans.*, 2014, **43**, 3906.

20 E. Collet, M. L. Boillot, J. Hebert, N. Moisan, M. Servol, M. Lorenc, L. Toupet, M. Buron-Le Cointe, A. Tissot and J. Sainton, *Acta Crystallogr., Sect. B: Struct. Sci.*, 2009, **65**, 474–480.
21 C. Faulmann, P. Á. Szilágyi, K. Jacob, J. Chahine and L. Valade, *New J. Chem.*, 2009, **33**, 1268.
22 A. B. Gaspar, M. C. Muñoz, N. Moliner, V. Ksenofontov, G. Levchenko, P. Gütlich and J. A. Real, *Monatsh. Chem.*, 2003, **134**, 285–294.
23 H. Hagiwara and S. Okada, *Chem. Commun.*, 2015, **52**, 815–818.
24 V. Legrand, S. Pechev, J.-F. Létard and P. Guionneau, *Phys. Chem. Chem. Phys.*, 2013, **15**, 13872–13880.
25 J. Luan, J. Zhou, Z. Liu, B. Zhu, H. Wang, X. Bao, W. Liu, M. L. Tong, G. Peng, H. Peng, L. Salmon and A. Bousseksou, *Inorg. Chem.*, 2015, **54**, 5145–5147.
26 G. S. Matouzenko, E. Jeanneau, A. Yu Verat and A. Bousseksou, *Dalton Trans.*, 2011, **40**, 9608–9618.
27 R. Pritchard, H. Lazar, S. A. Barrett, C. A. Kilner, S. Asthana, C. Carbonera, J.-F. Létard and M. A. Halcrow, *Dalton Trans.*, 2009, 6656.
28 D. L. Reger, J. R. Gardinier, M. D. Smith, A. M. Shahin, G. J. Long, L. Rebbouh and F. Grandjean, *Inorg. Chem.*, 2005, **44**, 1852–1866.
29 T. M. Ross, B. Moubaraki, S. M. Neville, S. R. Batten and K. S. Murray, *Dalton Trans.*, 2012, **41**, 1512.
30 C. F. Sheu, S. Pillet, Y. C. Lin, S. M. Chen, I. J. Hsu, C. Lecomte and Y. Wang, *Inorg. Chem.*, 2008, **47**, 10866–10874.
31 A. L. Thompson, A. E. Goeta, J. A. Real, A. Galet and M. Carmen Muñoz, *Chem. Commun.*, 2004, 1390–1391.
32 A. Lennartson, A. D. Bond, S. Piligkos and C. J. McKenzie, *Angew. Chem., Int. Ed.*, 2012, **51**, 11049–11052.
33 A. Arroyave, A. Lennartson, A. Dragulescu-Andrasi, K. S. Pedersen, S. Piligkos, S. A. Stoian, S. M. Greer, C. Pak, O. Hietsoi, H. Phan, S. Hill, C. J. McKenzie and M. Shatruk, *Inorg. Chem.*, 2016, **55**, 5904–5913.
34 P. Guionneau, M. Marchivie, G. Bravic, J.-F. Létard and D. Chasseau, *Top. Curr. Chem.*, 2004, **234**, 97–128.
35 M. Marchivie, P. Guionneau, J.-F. Létard and D. Chasseau, *Acta Crystallogr., Sect. B: Struct. Sci.*, 2005, **61**, 25–28.
36 J. Zhou, B.-W. Zhu, J. Luan, Z. Liu, J.-K. Fang, X. Bao, G. Peng, J. Tucek, S.-S. Bao and L.-M. Zheng, *Dalton Trans.*, 2015, **44**, 20551–20561.
37 X. Liu, J. Zhou, X. Bao, Z. Yan, G. Peng, M. Rouzières, C. Mathonière, J.-L. Liu and R. Clérac, *Inorg. Chem.*, 2017, **56**, 12148–12157.
38 T. Ueno, Y. Ii, T. Fujinami, N. Matsumoto, S. Iijima and Y. Sunatsuki, *Polyhedron*, 2017, **136**, 13–22.
39 L. B. Munro and V. J. Catalano, *Eur. J. Inorg. Chem.*, 2014, 4994–5007.
40 G. M. Sheldrick, *Acta Crystallogr., Sect. A: Found. Crystallogr.*, 2008, **64**, 112–122.
41 O. V. Dolomanov, L. J. Bourhis, R. J. Gildea, J. A. K. Howard and H. Puschmann, *J. Appl. Crystallogr.*, 2009, **42**, 339–341.